Skeletal Radiology
https://doi.org/10.1007/s00256-022-04192-5

SCIENTIFIC ARTICLE

Ultrafast lumbar spine MRI protocol using deep learning–based reconstruction: diagnostic equivalence to a conventional protocol

Masahiro Fujiwara[1] · Nobuo Kashiwagi[2] · Chisato Matsuo[3] · Hitoshi Watanabe[4] · Yoshimori Kassai[5] · Atsushi Nakamoto[6] · Noriyuki Tomiyama[3]

Received: 19 July 2022 / Revised: 23 September 2022 / Accepted: 23 September 2022

Abstract

Objective To evaluate the diagnostic equivalency between an ultrafast (1 min 53 s) lumbar MRI protocol using deep learning–based reconstruction and a conventional lumbar MRI protocol (12 min 31 s).

Materials and methods This study included 58 patients who underwent lumbar MRI using both conventional and ultrafast protocols, including sagittal T1-weighted, T2-weighted, short-TI inversion recovery, and axial T2-weighted sequences. Compared with the conventional protocol, the ultrafast protocol shortened the acquisition time to approximately one-sixth. To compensate for the decreased signal-to-noise ratio caused by the acceleration, deep learning–based reconstruction was applied. Three neuroradiologists graded degenerative changes and analyzed for presence of other pathologies. For the grading of degenerative changes, interprotocol intrareader agreement was assessed using kappa statics. Interchangeability between the two protocols was also tested by calculating the individual equivalence index between the intraprotocol interreader agreement and interprotocol interreader agreement. For the detection of other pathologies, interprotocol intrareader agreement was assessed.

Results For the grading of degenerative changes, the kappa values for interprotocol intrareader agreement of all three readers ranged from 0.707 to 0.804, indicating substantial to almost perfect agreement. Except for foraminal stenosis and disc contour on axial images, the 95% confidence interval of the individual equivalence index was < 5%, indicating the two protocols were interchangeable. For the detection of other pathologies, the interprotocol intrareader agreement rates were > 98% for each individual pathology.

Conclusions Our proposed ultrafast lumbar spine MRI protocol provided almost equivalent diagnostic results to that of the conventional protocol, except for some degenerative changes.

Keywords Lumbar spine · Magnetic resonance imaging · Fast imaging · Diagnostic performance · Deep learning

Introduction

Magnetic resonance imaging (MRI) is arguably the most powerful imaging modality for spinal disorders because of the high image contrast, variety of contrast mechanisms, and lack of exposure to ionizing radiation. However, its relatively long acquisition time, due to a trade-off relationship between the acquisition time and image quality, limits its clinical use in time-critical conditions and uncooperative patients.

To address this issue, which has existed since the advent of MRI, recent popular approaches include parallel imaging, compressed sensing, and synthetic method [1–3]. Applying these techniques to lumbar spine MRI, the total acquisition time of lumbar spine MRI can be reduced to approximately 5 min with image quality preservation comparable to that

✉ Nobuo Kashiwagi
nobuo.kashiwagi@oici.jp

1 Department of Diagnostic Radiology, Osaka Medical and Pharmaceutical University, Osaka, Japan

2 Department of Diagnostic and Interventional Radiology, Osaka International Cancer Institute, 〒541-8567 3-1-69 Otemae, Chuo-ku, Osaka 541-8567, Japan

3 Diagnostic and Interventional Radiology, Osaka University Graduate School of Medicine, Osaka, Japan

4 Department of Radiology, Yukoukai General Hospital, Osaka, Japan

5 Canon Medical Systems Corporation, Tochigi, Japan

6 Department of Future Diagnostic Radiology, Osaka University Graduate School of Medicine, Osaka, Japan

Published online: 01 October 2022

of conventional protocols [4–6]. More recently, deep learning, which has been increasingly applied to various areas of medical imaging, is now being used to reduce the acquisition time of MRI. In some preliminary studies, noise reduction using deep learning–based reconstruction (DLR) can reduce 45–60% of the acquisition time of spine MRI with image quality preservation, resulting in a total acquisition time of approximately 5 min [7, 8].

Another MRI acceleration approach from the viewpoint of preserving practical diagnosis without regard for preserving image quality, superfast brain MRI protocols with a total acquisition time of 1–3 min have been proposed. These brain MRI protocols were suggested to be a feasible option in specific clinical situations, such as in time-critical diseases or with motion-prone patients [9–12].

Consequently, we hypothesized that an ultrafast spine MRI protocol might be possible by combining the following factors: (i) applying a recently emerged noise reduction technique using DLR, and (ii) focusing not on the image quality but on the practical diagnostic performance. In the current study, we proposed a novel ultrafast lumbar MRI protocol with a total acquisition time of < 2 min and compared the image interpretation of this ultrafast protocol with that of a conventional protocol.

Materials and methods

Patients

The protocol for this study was approved by the institutional review board, and all included patients provided written informed consent. Among 141 consecutive patients who had indications for lumbar MRI examination between August 2020 and December 2020, 58 who agreed to participate in this study were enrolled. This included 24 men and 34 women with a mean age of 66 (range, 21–91) years. The reasons for performing lumbar MRI were lower extremity pain in 28, back pain in 20, lower extremity numbness in seven, and lower limb muscle weakness in three patients.

MRI data acquisition

We performed lumbar MRI examinations using a 1.5 T MRI scanner (Vantage Orian™ 1.5 T, Canon Medical Systems Corporation, Tochigi, Japan) with a 32-element phased-array surface spine coil. All patients underwent conventional and ultrafast protocols, and both protocols included four sequences (sagittal T1-weighted and T2-weighted, short-TI inversion recovery [STIR], and axial T2-weighted sequences). Detailed MRI acquisition parameters are listed in Table 1. Under the supervision of MRI technicians, the acquisition time of the ultrafast protocol was shortened by using a lower number of excitations, lower oversampling rate, application of compressed sensing, and lower spatial resolution than those of the conventional protocol. As a result, the total scan time of the ultrafast protocol was reduced to 1 min 53 s, while that of the conventional protocol was 12 min 31 s. We applied a commercialized denoising method using DLR (Advanced Intelligent Clear-IQ Engine [AiCE], Canon Medical Systems Corporation, Tochigi, Japan) to compensate for the reduced image quality caused by the shortened acquisition time in the ultrafast protocol. Several previous studies have confirmed that this DLR can

Table 1 Comparison of acquisition parameters between the ultrafast and conventional protocols

	Conv	Ultra	Conv	Ultra	Conv	Ultra	Conv	Ultra
Sequence	Sagittal T1WI		Sagittal T2WI		Sagittal STIR		Axial T2WI	
TR (ms)	566	500	4000	3010	5100	4450	4000	
TE (ms)	10		90		80		120	
Echo train length	2		17		17		23	
Slice thickness (mm)	3	4	3	4	3	4	4	4
FOV phase (mm)	300		300		300		180	
FOV read (mm)	270		270		270		180	
Matrix (phase)	288	192	352	192	224	192	288	192
Matrix (read)	356		320		320		320	256
Oversampling (%)	100	50	100	50	50		100	50
NEX	1	1	1	1	2	1	2	1
Acceleration factor in CS	None	3	None	3	None	3	None	2
Acquisition time (min:s)	2:45	0:26	2:52	0:19	3:30	0:32	3:24	0:36

The total acquisition time was 12 min 31 s for the conventional protocol and 1 min 53 s for the ultrafast protocol

WI, weighted image; *Conv*, conventional; *Ultra*, ultrafast; *TR*, repetition time; *TE*, echo time; *FOV*, field of view; *CS*, compressed sensing; *NEX*, number of excitations; *STIR*, short-TI inversion recovery

improve the signal-to-noise ratio of normal tissue in various MRI sequences and at various anatomic sites [8, 13–15].

Image interpretation

Three neuroradiologists (6, 11, and 25 years of experience in neuroradiology, respectively), who were blinded to the clinical information, independently evaluated the grading of lumbar degenerative changes and the presence of other pathologies. First, the images obtained from the conventional protocol were evaluated, followed by the evaluation of the images obtained from the ultrafast protocol. The order of cases in each evaluation session was randomized, and the interval between the two evaluation sessions was set at 4 weeks to minimize recall bias [16, 17].

MRI criteria for degenerative change

Based on the following classifications from the literature, degenerative changes included central canal stenosis on axial images, foraminal stenosis on sagittal images, lumbar disc contour on axial and sagittal images, lumbar disc nucleus degeneration on sagittal images, and endplate degeneration on sagittal images.

- Central canal stenosis (four grades): grade 0, no stenosis; grade 1, mild cerebrospinal fluid space stenosis with clear separation of each nerve root in the cauda equina; grade 2, moderate stenosis with some aggregation within the cauda equina; grade 3, severe stenosis with complete aggregation, where the nerve roots cannot be separated from each other [18].
- Foraminal stenosis (four grades): grade 0, normal; grade 1, perineural fat obliteration surrounding the nerve root in one or two directions; grade 2, perineural fat obliteration surrounding the nerve root in four directions with no collapse or morphologic change of the nerve root; grade 3, nerve root collapse or morphologic changes due to severe foraminal stenosis [19].
- Disc contour on axial images (five grades): grade 0, normal; grade 1, bulging (circumferential extension of disc material beyond the intervertebral disc space, "circumferential" is defined as > 25% of the disc circumference); grade 2, protrusion (focal extension of the disc material, "focal" is defined as < 25% of the disc circumference); grade 3, extrusion (focal extension of the disc material with the greatest measure of the displaced disc being greater than the base of the displaced disc); grade 4, sequestration (no continuity between displaced disc material and disc of origin) [20, 21].
- Disc contour on sagittal images (five grades): grade 0, normal disc; grade 1, diffuse bulging (circumferential, symmetric disc extension beyond the vertebral border); grade 2, protrusion (a focal or asymmetric extension of the disc beyond the vertebral border, with the disc origin being broader than any other dimension of the protrusion); grade 3, extrusion (a more extreme extension of the disc beyond the vertebral border, with the diameter of the extruding material being greater than the base of the displaced material at the disc space of origin); grade 4, sequestration (a free disc fragment distinct from the parent disc) [20, 21].
- Lumbar disc nucleus degeneration (seven grades): grade 0, bright (normal); grade 1, bright band (normal disc height and hyperintense nucleus signal with dark horizontal band); grade 2, bright-narrow (decreased disc height and hyperintense nucleus signal with or without dark horizontal band); grade 3, dim (normal disc height and decreased nucleus signal with slight or heterogeneous irregularity); grade 4, dim-slight (slightly decreased disc height and decreased nucleus signal with slight or heterogeneous irregularity); grade 5, dim-moderate (moderately decreased disc height and decreased nucleus signal with moderately); grade 6, dim-collapsed (collapsed disc height and hypointense nucleus signal) [22].
- Endplate degeneration (four types): type 0, normal; type 1, inflammatory changes (hypointense on T1WI and hyperintense on STIR); type 2, fatty changes (hyperintense on T1WI and hypointense on STIR); and type 3, fibrous changes (hypointense on T1WI and STIR) [23].

Other pathologies

The readers also recorded the presence or absence of pathologies other than degenerative changes. Pathologies outside the spinal column were removed from the scope of the evaluation.

Statistical analysis

Grading of degenerative changes—Cohen's kappa statistics

Using linear weighted kappa statistics, the interprotocol intrareader agreement of the three readers was evaluated for all variables, except for endplate degeneration, where we used unweighted kappa statistics because it was measured on a nominal scale. Kappa values were interpreted using Landis and Koch's categorization: 0–0.20, slight agreement; 0.21–0.40, fair agreement; 0.41–0.60, moderate agreement; 0.61–0.80, substantial agreement; and 0.81–1.00, almost perfect agreement [24].

Grading of degenerative changes—interchangeability

We also verified interchangeability between the two protocols because there is no reference standard for degenerative

changes. Interchangeability is a method of evaluating whether a new imaging technique can replace an existing one by ensuring that the agreement rate when one of the readers uses the new imaging technique is not significantly lower than that of the agreement rate when both readers use the existing imaging technique [16, 17, 25]. First, we calculated the rate of intraprotocol interreader agreement (both readers evaluated the conventional images) and interprotocol interreader agreement (one reader evaluated the conventional images, and the other evaluated the ultrafast images) for each variable. Then, the individual equivalence index was calculated as the estimated difference by subtracting the interprotocol interreader agreement rate from the intraprotocol interreader agreement rate; a 95% confidence interval (CI) for the difference was constructed by performing bootstrapping methods with 1000 repetitions. The interchangeability of the two protocols was defined as the upper bound of 95% CI of the individual equivalence index < 5%.

Detection of other pathologies

For each pathology, we calculated the interprotocol intrareader agreement rates.

Results

Grading of degenerative changes—Cohen's kappa values

The kappa values of the interprotocol intrareader agreement for all three readers ranged from 0.707 to 0.804, indicating substantial to almost perfect agreement. For each reader, the interprotocol intrareader agreement was also substantial to almost perfect, except for the endplate degeneration of one reader, which was moderate. The detailed kappa values of each reader are shown in Table 2. Representative cases are shown in Figs. 1, 2, and 3.

Grading of degenerative changes—interchangeability

Intraprotocol (conventional vs. conventional) interreader agreement, interprotocol (conventional vs. ultrafast) interreader agreement, and 95% CI of the individual equivalence index are shown in Table 3. The upper bounds of the 95% CI for central canal stenosis, disc contour on

Table 2 Interprotocol intrareader agreement for the grading of degenerative changes

	Reader	kappa value	95% CI	Agreement rate
Central canal stenosis	Reader 1	0.765	0.699–0.831	235/284 (82.7%)
	Reader 2	0.867	0.818–0.916	258/284 (90.8%)
	Reader 3	0.755	0.685–0.825	244/284 (85.9%)
	All	0.804	0.769–0.838	737/852 (86.5%)
Foraminal stenosis	Reader 1	0.738	0.674–0.802	509/580 (87.9%)
	Reader 2	0.836	0.791–0.880	527/580 (90.9%)
	Reader 3	0.641	0.585–0.700	461/580 (79.5%)
	All	0.736	0.703–0.768	1498/1740 (86.1%)
Disc contour axial	Reader 1	0.726	0.650–0.802	238/284 (83.8%)
	Reader 2	0.860	0.807–0.913	258/284 (90.8%)
	Reader 3	0.645	0.572–0.719	212/284 (74.6%)
	All	0.758	0.721–0.794	708/852 (83.1%)
Disc contour sagittal	Reader 1	0.720	0.658–0.782	220/290 (75.9%)
	Reader 2	0.902	0.867–0.937	261/290 (90.0%)
	Reader 3	0.667	0.594–0.740	220/290 (75.9%)
	All	0.776	0.743–0.808	700/870 (80.5%)
Disc degeneration	Reader 1	0.760	0.714–0.806	195/288 (67.7%)
	Reader 2	0.879	0.842–0.916	245/288 (85.1%)
	Reader 3	0.670	0.605–0.736	202/288 (70.1%)
	All	0.773	0.743–0.803	642/864 (74.3%)
Endplate degeneration	Reader 1	0.649	0.548–0.750	256/290 (88.3%)
	Reader 2	0.863	0.802–0.925	273/290 (94.1%)
	Reader 3	0.579	0.480–0.678	244/290 (84.1%)
	All	0.707	0.655–0.759	773/870 (88.9%)

All variables were calculated using linear weighted Cohen's kappa statistics, except for endplate degeneration, which was calculated using unweighted Cohen's kappa statistics

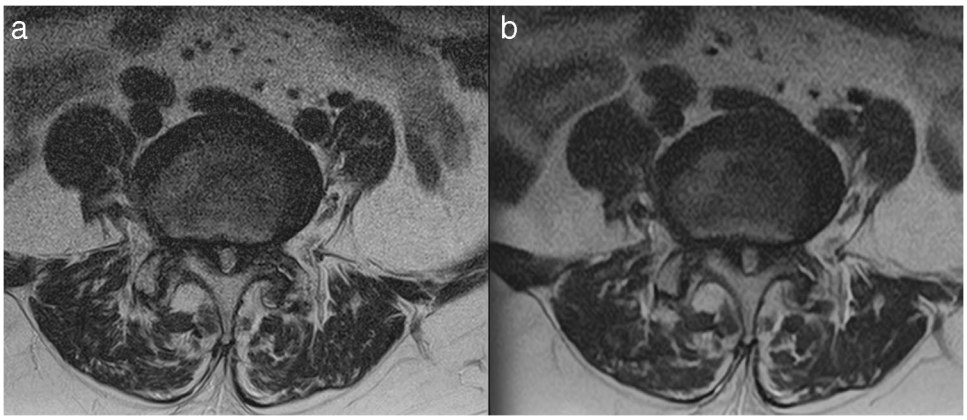

Fig. 1 A 76-year-old woman with bilateral buttock pain. Axial conventional (**a**) and ultrafast (**b**) T2-weighted images at L4-5 disc. All readers graded the findings as severe (grade 3) central canal stenosis in both protocols

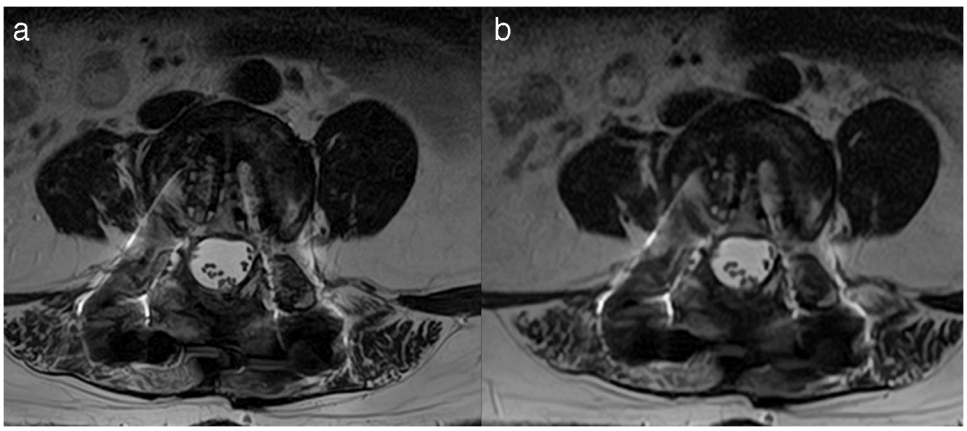

Fig. 2 A 79-year-old woman with a follow-up examination of posterior lumbar intervertebral body fusion. Axial conventional (**a**) and ultrafast (**b**) T2-weighted images at L3-4 disc. All readers graded the findings as no (grade 0) central canal stenosis and normal (grade 0) disc contour in both protocols

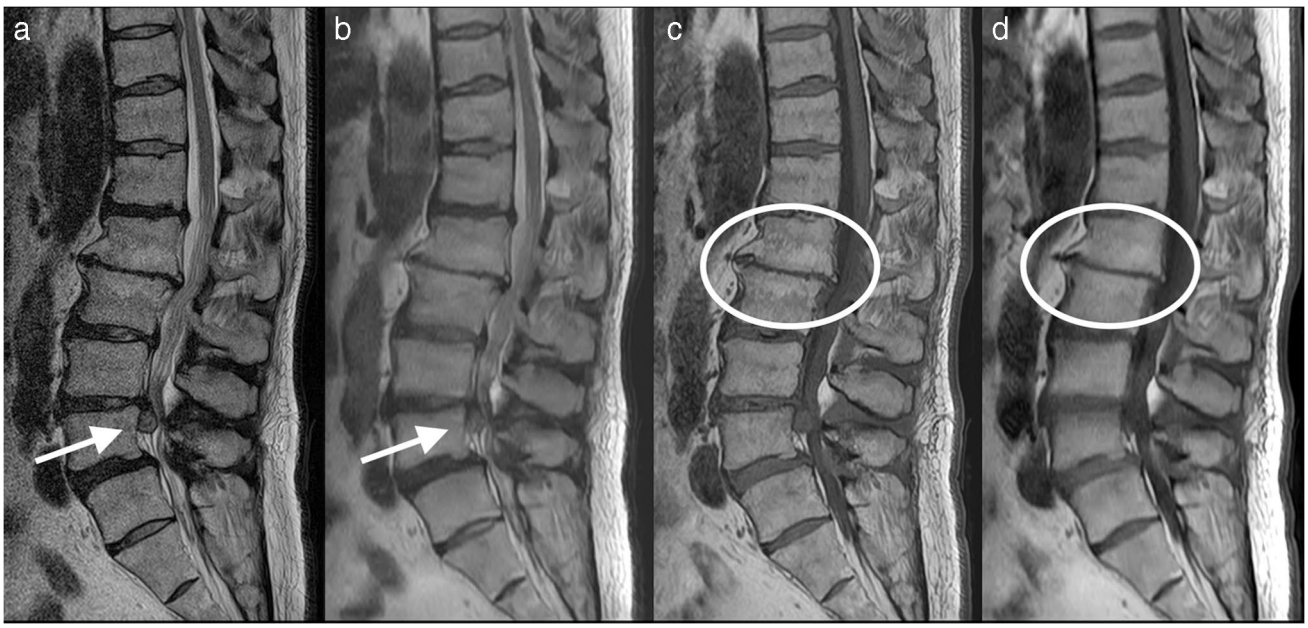

Fig. 3 A 65-year-old man with intermittent claudication. Sagittal conventional T2-weighted (**a**), ultrafast T2-weighted (**b**), conventional T1-weighted (**c**), and ultrafast T1-weighted (**d**) images. All readers graded the L3-4 disc as an extrusion (arrows), and classified the L1 and L2 endplate degenerations as Modic type 2 (circle) in both protocols

Table 3 Interchangeability: intraprotocol interreader and interprotocol interreader agreement rates and 95% confidence interval of the individual equivalence index

Variable	Interreader agreement rate
Central canal stenosis	
Intraprotocol (conventional vs. conventional)	589/852 (69.13%)
Interprotocol (conventional vs. ultrafast)	1207/1704 (70.83%)
95% CI of the individual equivalence index (%)	−5.28 to 2.11
Foraminal stenosis	
Intraprotocol (conventional vs. conventional)	1509/1740 (86.72%)
Interprotocol (conventional vs. ultrafast)	2826/3480 (81.21%)
95% CI of the individual equivalence index (%)	3.56 to 7.39
Disc contour on axial images	
Intraprotocol (conventional vs. conventional)	531/852 (62.32%)
Interprotocol (conventional vs. ultrafast)	1031/1704 (60.50%)
95% CI of the individual equivalence index (%)	−2.23 to 5.58
Disc contour on sagittal images	
Intraprotocol (conventional vs. conventional)	519/870 (59.66%)
Interprotocol (conventional vs. ultrafast)	1077/1740 (61.90%)
95% CI of the individual equivalence index (%)	−5.92 to 1.67
Disc degeneration	
Intraprotocol (conventional vs. conventional)	564/864 (65.28%)
Interprotocol (conventional vs. ultrafast)	1135/1728 (65.68%)
95% CI of the individual equivalence index (%)	−4.52 to 3.36
Endplate degeneration	
Intraprotocol (conventional vs. conventional)	725/870 (83.33%)
Interprotocol (conventional vs. ultrafast)	1439/1740 (82.70%)
95% CI of the individual equivalence index (%)	−2.18 to 3.56

Interreader agreement rates are shown as number of agreements/total number (%)

95% confidence interval (CI) is shown for the individual equivalence index (intraprotocol interreader agreement minus interprotocol interreader agreement)

sagittal images, disc degeneration, and endplate degeneration were within 5%, indicating that the two protocols are interchangeable. Those for foraminal stenosis and disc contour on axial images were slightly higher than 5%, 7.39%, and 5.58%, respectively.

Detection of other pathologies

Other pathologies were noted in 12 of the 58 patients. These included fresh compression fractures in eight patients, old compression fractures in six patients, and vertebral tumors in two patients. Agreement rates of all readers were > 98% for each pathology. Details on the interprotocol intrareader agreements in diagnosing other pathologies are shown in Table 4. The interprotocol intrareader disagreements were noted in two readers on the same vertebra with old compression fracture. Representative cases are shown in Figs. 4 and 5.

Discussion

In this study, we evaluated the diagnostic equivalence between our proposed ultrafast protocol and the conventional protocol for lumbar spine MRI. Regarding the evaluation of degenerative changes, the kappa statistics indicated substantial to almost perfect interprotocol intrareader agreement for all variables. In addition, the calculation of the individual equivalence index indicated that both protocols were interchangeable, except for the degree of foraminal stenosis and disc contour on axial images. Regarding the detection of other pathologies, interprotocol intrareader agreement rates were > 98%. Based on these results, our proposed ultrafast lumbar spine protocol can be a practical option for patients who need a short examination time, such as those with medical emergencies, difficulty lying still for long periods because of back pain or other reasons, and pediatric patients requiring sedation.

Table 4 Interprotocol intrareader agreement for the detection of other pathologies

		Agreement rate	Number of positive pairs	Number of discordant pairs
Fresh compression fracture	Reader 1	58/58 (100%)	8	0
	Reader 2	58/58 (100%)	7	0
	Reader 3	58/58 (100%)	8	0
	All	174/174 (100%)	23	0
Old compression fracture	Reader 1	57/58 (98.3%)	5	1
	Reader 2	58/58 (100%)	6	0
	Reader 3	57/58 (98.3%)	6	1
	All	172/174 (98.9%)	17	2
Tumor	Reader 1	58/58 (100%)	1	0
	Reader 2	58/58 (100%)	1	0
	Reader 3	58/58 (100%)	2	0
	All	174/174 (100%)	4	0

Agreement rates are shown as the number of patients with an agreed number/total number of patients (%)

The number of positive pairs refers to the number of patients found to have other pathologies in both protocols

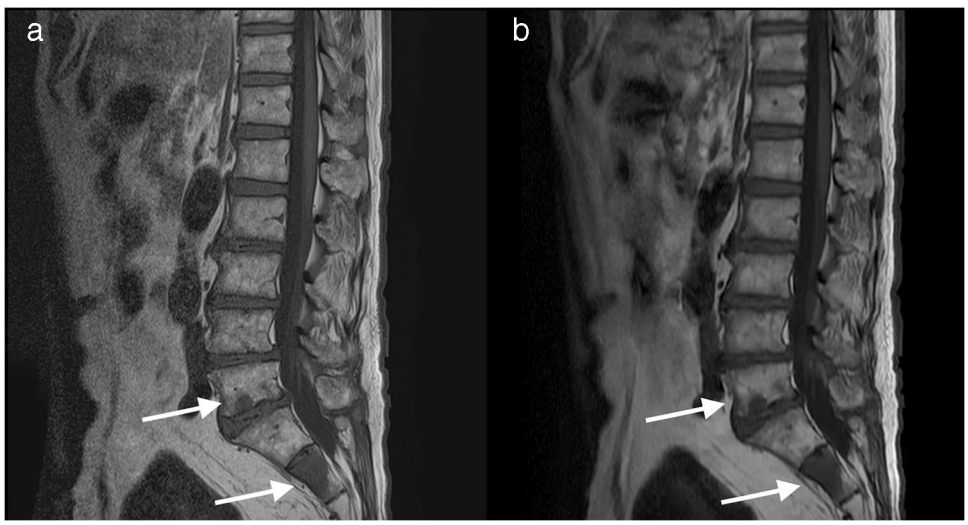

Fig. 4 A 90-year-old man with lumbago. Sagittal conventional (**a**) and ultrafast (**b**) T1-weighted images. These images demonstrate multiple vertebral tumors with comparable lesion conspicuity. Increased serum prostate-specific antigen levels with a history of prostate cancer resulted in a clinical diagnosis of multiple vertebral metastases

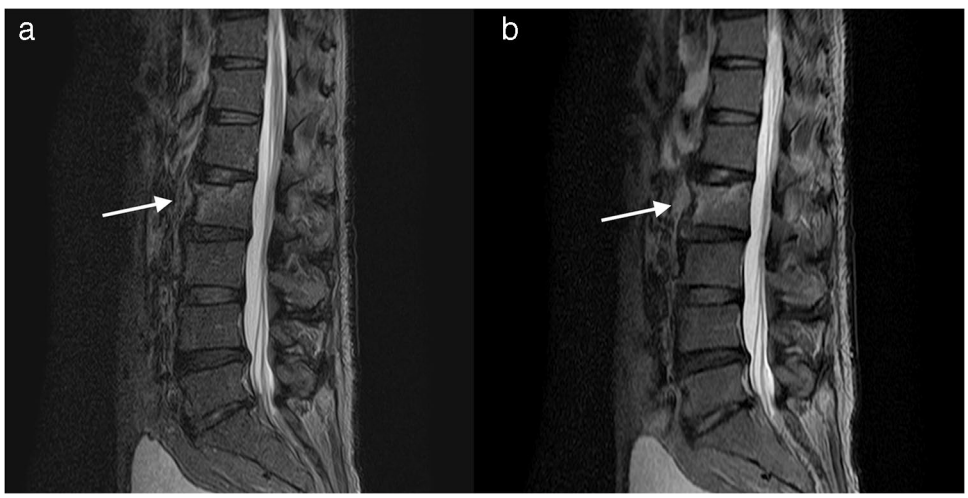

Fig. 5 A 68-year-old man with continuous back pain for 2 weeks. Conventional (**a**) and ultrafast (**b**) sagittal short-TI inversion recovery images. Mild decompression of the superior L2 endplate with bone marrow hyperintensity visible in both protocols. All readers detected fresh compression fracture of L2 in both protocols

The diagnostic equivalency between the ultrafast and conventional MRI protocols on many evaluation items may have the following two implications.

First, the denoising method using DLR did not compromise the pathological information. A major concern with usual denoising techniques for MRI is the loss of structural information affecting diagnostic performance [26]. The denoising method used in this study has been validated to improve image quality or reduce the acquisition time of MRI on various anatomical sites [8, 13–15]; however, its influence on pathologies has not yet been fully evaluated. Therefore, our data could be a useful reference for further applications of the denoising method to clinical MR examination. Second, there is a discrepancy between the image quality and diagnostic performance. Previous studies on brain MRI have reported that reduction in image quality preceded the loss of diagnostic efficacy [12, 27]. Although the evaluation of image quality is beyond the scope of our study, we assume that the deterioration of image quality in our ultrafast protocol did not affect image interpretation, except for grading some degenerative changes. As a future challenge, it would be worthwhile to know if the degree of image quality is commensurate with the diagnostic performance required in clinical practice.

In contrast to many other variables of lumbar degenerative changes, the upper bounds of the 95% CI of the individual equivalence index for foraminal stenosis and disc contour on axial images were > 5%, indicating that interchangeability could not be confirmed for these two variables. As for foraminal stenosis, the relatively high disagreement between the two protocols can be explained by the lower spatial resolution of the ultrafast protocol. Since the main criterion for grading foraminal stenosis is the degree of perineural fat obliteration, we speculated that the relatively lower spatial resolution on the superfast protocol can obscure thinned fat layer, resulting in a discrepancy between image interpretations of the two protocols. Clinically, it has been reported that the grade of foraminal stenosis on MRI correlates with a neurologic presentation [28, 29], which indicates that our proposed ultrafast protocol cannot completely replace the conventional protocol. Therefore, in the actual operation of the ultrafast protocol, one option may be to increase the spatial solution of T1-weighted sagittal images to the same level as that of the conventional protocol.

As for disc contour on axial images, the inherent lower interreader agreement compared with other degenerative changes, as reported in a previous study, may have affected the interchangeability between the two protocols [30]. The main reason for the low interreader agreement of grading disc contour was reported in the "bulging" category [31–33]; however, the bulging disc has low clinical significance because it is assumed to be an asymptomatic lesion [22, 34]. Therefore, considering that the upper bound of the 95% CI for disc contour on axial images was only slightly above 5% (5.58%), its clinical influence may be minimal.

This study had some limitations. First, this study had a relatively small number of participants, limiting the number of pathologies detected other than degenerative changes. Therefore, the diagnostic equivalence for other pathologies could not be adequately evaluated. Further studies in larger populations with various pathologies are warranted. Second, the readers could not be blinded to the protocol during image evaluation because the difference in image quality between the two protocols was obvious. However, we believe the researcher bias is minimal since the image interpretation in this study was not an evaluation of the degree of image quality or diagnostic confidence level, but rather the grading of degenerative changes and detection of other pathologies in the absence of a reference standard. Third, we set the minimum reading interval between the two protocols at 4 weeks based on previous studies [16, 17]; however, there may still be room for recall bias. Finally, the protocol acceleration was performed using a specific 1.5 T machine and was not fully validated with respect to its optimization. Therefore, a further study involving setting up a similar ultrafast protocol in other MRI systems, its optimization, and evaluation of its diagnostic performance will validate the results of this study.

Conclusion

Our proposed ultrafast lumbar spine MRI protocol resulted in almost identical image interpretation by radiologists to that of the conventional protocol, except for grading foraminal stenosis and disc contour on axial images.

Acknowledgements We thank Hiroyuki Kurakami, PhD (Data Coordinating Center, Department of Medical Innovation, Osaka University Hospital), for assisting us with the statistical analysis.

Declarations

Conflict of interest Yoshimori Kassai is an employee of the Canon Medical Systems Corporation.

References

1. Lockner JF, Hu HH, Stanley DW, Angelos L, King K. Parallel MR imaging: a user's guide. Radiographics. 2005;25(5):1279–97. https://doi.org/10.1148/rg.255045202.
2. Jaspan ON, Fleysher R, Lipton ML. Compressed sensing MRI: a review of the clinical literature. Br J Radiol. 2015;88(1056):20150487. https://doi.org/10.1259/bjr.20150487.
3. Ji S, Yang D, Lee J, Choi SH, Kim H, Kang KM. Synthetic MRI: technologies and applications in neuroradiology. J Magn Reson Imaging. 2022;55(4):1013–25. https://doi.org/10.1002/jmri.27440.

4. Vargas MI, Drake-Pérez M, Delattre BMA, Boto J, Lovblad KO, Boudabous S. Feasibility of a synthetic MR imaging sequence for spine imaging. AJNR Am J Neuroradiol. 2018;39:1756–63.
5. Longo MG, Fagundes J, Huang S, et al. Simultaneous multislice-based 5-minute lumbar spine MRI protocol: initial experience in a clinical setting. J Neuroimaging. 2017;27(5):442–6.
6. Qiu J, Liu J, Bi Z, et al. An investigation of 2D spine magnetic resonance imaging (MRI) with compressed sensing (CS). Skeletal Radiol. 2022;51:1273–83.
7. Bash S, Johnson B, Gibbs W, Zhang T, Shankaranarayanan A, Tanenbaum LN. Deep learning image processing enables 40% faster spinal MR scans which match or exceed quality of standard of care: a prospective multicenter multireader study. Clin Neuroradiol. 2022;32(1):197–203.
8. Kashiwagi N, Tanaka H, Yamashita Y, et al. Applicability of deep learning-based reconstruction trained by brain and knee 3T MRI to lumbar 1.5T MRI. Acta Radiol Open. 2021;10:20584601211023940.
9. Ha JY, Baek HJ, Ryu KH, et al. One-minute ultrafast brain MRI with full basic sequences: can it be a promising way forward for pediatric neuroimaging? AJR Am J Roentgenol. 2020;215:198–205.
10. Ryu KH, Baek HJ, Skare S, et al. Clinical experience of 1-minute brain MRI using a multicontrast EPI sequence in a different scan environment. AJNR Am J Neuroradiol. 2020;41(3):424–9.
11. Ryu KH, Choi DS, Baek HJ, et al. Clinical feasibility of 1-min ultrafast brain MRI compared with routine brain MRI using synthetic MRI: a single center pilot study. J Neurol. 2019;266(2):431–9.
12. U-King-Im JM, Trivedi RA, Graves MJ, et al. Utility of an ultrafast magnetic resonance imaging protocol in recent and semi-recent strokes. J Neurol Neurosurg Psychiatry. 2005;76(7):1002–5.
13. Kidoh M, Shinoda K, Kitajima M, et al. Deep learning based noise reduction for brain MR imaging: tests on phantoms and healthy volunteers. Magn Reson Med Sci. 2020;19:195–206.
14. Uetani H, Nakaura T, Kitajima M, et al. A preliminary study of deep learning-based reconstruction specialized for denoising in high-frequency domain: usefulness in high-resolution three-dimensional magnetic resonance cisternography of the cerebellopontine angle. Neuroradiology. 2021;63:63–71.
15. Ueda T, Ohno Y, Yamamoto K, et al. Compressed sensing and deep learning reconstruction for women's pelvic MRI denoising: utility for improving image quality and examination time in routine clinical practice. Eur J Radiol. 2021;134:109430.
16. Alaia EF, Benedick A, Obuchowski NA, et al. Comparison of a fast 5-min knee MRI protocol with a standard knee MRI protocol: a multi-institutional multi-reader study. Skeletal Radiol. 2018;47:107–16.
17. Zanchi F, Richard R, Hussami M, Monier A, Knebel JF, Omoumi P. MRI of non-specific low back pain and/or lumbar radiculopathy: do we need T1 when using a sagittal T2-weighted Dixon sequence? Eur Radiol. 2020;30:2583–93.
18. Lee GY, Lee JW, Choi HS, Oh KJ, Kang HS. A new grading system of lumbar central canal stenosis on MRI: an easy and reliable method. Skelet Rad. 2011;40:1033–9.
19. Lee S, Lee JW, Yeom JS, et al. A practical MRI grading system for lumbar foraminal stenosis. AJR Am J Roentgenol. 2010;194:1095–8.
20. Macki M, Hernandez-Hermann M, Bydon M, Gokaslan A, McGovern K, Bydon A. Spontaneous regression of sequestrated lumbar disc herniations: literature review. Clin Neurol Neurosurg. 2014;120:136–41.
21. Fardon DF, Williams AL, Dohring EJ, Murtagh FR, Gabriel Rothman SL, Sze GK. Lumbar disc nomenclature: version 2.0: recommendations of the combined task forces of the North American Spine Society, the American Society of Spine Radiology and the American Society of Neuroradiology. Spine J. 2014;14(11):2525–45.
22 Kim SJ, Lee TH, Lim SM. Prevalence of disc degeneration in asymptomatic Korean subjects. Part 1: lumbar spine. J Korean Neurosurg Soc. 2013;53:31–8.
23. Modic MT, Ross JS. Lumbar degenerative disk disease. Radiology. 2007;245:43–61.
24. Landis JR, Koch GG. The measurement of observer agreement for categorical data. Biometrics. 1977;33:159–74.
25. Obuchowski NA, Subhas N, Schoenhagen P. Testing for interchangeability of imaging tests. Acad Radiol. 2014;21:1483–9.
26. Mishro PK, Agrawal S, Panda R, Abraham A. A survey on state-of-the-art denoising techniques for brain magnetic resonance images. IEEE Rev Biomed Eng. 2022;15:184–99.
27. Terae S, Miyasaka K, Kudoh K, et al. Wavelet compression on detection of brain lesions with magnetic resonance imaging. J Digit Imaging. 2000;13:178–90.
28. Park HJ, Kim SS, Lee SY, et al. Clinical correlation of a new MR imaging method for assessing lumbar foraminal stenosis. AJNR Am J Neuroradiol. 2012;33(5):818–22.
29. Jeong TS, Ahn Y, Lee SG, Kim WK, Son S, Kwon JH. Correlation between MRI grading system and surgical findings for lumbar foraminal stenosis. J Korean Neurosurg Soc. 2017;60(4):465–70. https://doi.org/10.3340/jkns.2016.1010.004.
30. Doktor K, Jensen TS, Christensen HW, et al. Degenerative findings in lumbar spine MRI: an inter-rater reliability study involving three raters. Chiropr Man Therap. 2020;28(1):8.
31 Brant-Zawadzki MN, Jensen MC, Obuchowski N, Ross JS, Modic MT. Interobserver and intraobserver variability in interpretation of lumbar disc abnormalities. A comparison of two nomenclatures. Spine (Phila Pa 1976). 1995;20(11):1257–63. (discussion 1264).
32. van Rijn JC, Klemetsö N, Reitsma JB, et al. Observer variation in MRI evaluation of patients suspected of lumbar disk herniation. AJR Am J Roentgenol. 2005;184(1):299–303.
33. Hajiahmadi S, Shayganfar A, Askari M, Ebrahimian S. Interobserver and intraobserver variability in magnetic resonance imaging evaluation of patients with suspected disc herniation. Heliyon. 2020;6(11):e05201.
34. Jensen MC, Brant-Zawadzki MN, Obuchowski N, Modic MT, Malkasian D, Ross JS. Magnetic resonance imaging of the lumbar spine in people without back pain. N Engl J Med. 1994;331(2):69–73.